Quantitative OCT angiography of optic nerve head blood flow

Yali Jia,[1] John C. Morrison,[1] Jason Tokayer,[2] Ou Tan,[1] Lorinna Lombardi,[1] Bernhard Baumann,[3] Chen D. Lu,[3] WooJhon Choi,[3] James G. Fujimoto,[3] and David Huang[1,*]

[1]*Casey Eye Institute, Oregon Health & Science University, Portland, OR 97239, USA*
[2]*Department of Electrical Engineering, University of Southern California, Los Angeles, CA 90089, USA*
[3]*Department of Electrical Engineering and Computer Science, and Research Laboratory of Electronics, Massachusetts Institute of Technology, Cambridge, MA 02139, USA*
*huangd@ohsu.edu

Abstract: Optic nerve head (ONH) blood flow may be associated with glaucoma development. A reliable method to quantify ONH blood flow could provide insight into the vascular component of glaucoma pathophysiology. Using ultrahigh-speed optical coherence tomography (OCT), we developed a new 3D angiography algorithm called split-spectrum amplitude-decorrelation angiography (SSADA) for imaging ONH microcirculation. In this study, a method to quantify SSADA results was developed and used to detect ONH perfusion changes in early glaucoma. *En face* maximum projection was used to obtain 2D disc angiograms, from which the average decorrelation values (flow index) and the percentage area occupied by vessels (vessel density) were computed from the optic disc and a selected region within it. Preperimetric glaucoma patients had significant reductions of ONH perfusion compared to normals. This pilot study indicates OCT angiography can detect the abnormalities of ONH perfusion and has the potential to reveal the ONH blood flow mechanism related to glaucoma.

OCIS codes: (170.4500) Optical coherence tomography; (170.3880) Medical and biological imaging; (170.4470) Ophthalmology.

References and links

1. H. A. Quigley and S. Vitale, "Models of open-angle glaucoma prevalence and incidence in the United States," Invest. Ophthalmol. Vis. Sci. **38**(1), 83–91 (1997).
2. L. Hyman, S. Y. Wu, A. M. Connell, A. Schachat, B. Nemesure, A. Hennis, and M. C. Leske, "Prevalence and causes of visual impairment in The Barbados Eye Study," Ophthalmology **108**(10), 1751–1756 (2001).
3. B. L. Petrig, C. E. Riva, and S. S. Hayreh, "Laser Doppler flowmetry and optic nerve head blood flow," Am. J. Ophthalmol. **127**(4), 413–425 (1999).
4. S. S. Hayreh, "Blood supply of the optic nerve head and its role in optic atrophy, glaucoma, and oedema of the optic disc," Br. J. Ophthalmol. **53**(11), 721–748 (1969).
5. S. S. Hayreh, "Progress in the understanding of the vascular etiology of glaucoma," Curr. Opin. Ophthalmol. **5**(2), 26–35 (1994).
6. S. S. Hayreh, "Posterior ciliary artery circulation in health and disease: the Weisenfeld lecture," Invest. Ophthalmol. Vis. Sci. **45**(3), 749–757, 748 (2004).
7. J. François and J. J. de Laey, "Fluorescein angiography of the glaucomatous disc," Ophthalmologica **168**(4), 288–298 (1974).
8. S. S. Hayreh, "Colour and fluorescence of the optic disc," Ophthalmologica **165**(2), 100–108 (1972).
9. M. R. Stein and C. W. Parker, "Reactions following intravenous fluorescein," Am. J. Ophthalmol. **72**(5), 861–868 (1971).
10. B. L. Petrig and C. E. Riva, "Optic nerve head laser Doppler flowmetry: principles and computer analysis," in *Ocular Blood Flow. New Insights into the Pathogenesis of Ocular Diseases*, H. J. Kaiser, J. Flammer, and P. Hendrickson, eds. (Karger Basel, 1995), pp. 120–127.
11. C. E. Riva, "Basic principles of laser Doppler flowmetry and application to the ocular circulation," Int. Ophthalmol. **23**(4/6), 183–189 (2001).

12. C. P. Jonescu-Cuypers, H. S. Chung, L. Kagemann, Y. Ishii, D. Zarfati, and A. Harris, "New neuroretinal rim blood flow evaluation method combining Heidelberg retina flowmetry and tomography," Br. J. Ophthalmol. **85**(3), 304–309 (2001).
13. T. Sugiyama, M. Araie, C. E. Riva, L. Schmetterer, and S. Orgul, "Use of laser speckle flowgraphy in ocular blood flow research," Acta Ophthalmol. (Copenh.) **88**(7), 723–729 (2010).
14. J. R. Piltz-seymour, J. E. Grunwald, S. M. Hariprasad, and J. Dupont, "Optic nerve blood flow is diminished in eyes of primary open-angle glaucoma suspects," Am. J. Ophthalmol. **132**(1), 63–69 (2001).
15. G. Michelson, M. J. Langhans, and M. J. Groh, "Perfusion of the juxtapapillary retina and the neuroretinal rim area in primary open angle glaucoma," J. Glaucoma **5**(2), 91–98 (1996).
16. A. S. Hafez, R. L. G. Bizzarro, and M. R. Lesk, "Evaluation of optic nerve head and peripapillary retinal blood flow in glaucoma patients, ocular hypertensives, and normal subjects," Am. J. Ophthalmol. **136**(6), 1022–1031 (2003).
17. T. Sugiyama, M. Shibata, S. Kojima, and T. Ikeda, "Optic Nerve Head Blood Flow in Glaucoma," in The Mystery of Glaucoma, T. Kubena, ed. (InTech, 2011), pp. 207–218.
18. C. Prünte, J. Flammer, R. Markstein, and M. Rudin, "Quantification of optic nerve blood flow changes using magnetic resonance imaging," Invest. Ophthalmol. Vis. Sci. **36**(1), 247–251 (1995).
19. G. H. Garcia, K. M. Donahue, J. L. Ulmer, and G. J. Harris, "Qualitative perfusion imaging of the human optic nerve," Ophthal. Plast. Reconstr. Surg. **18**(2), 107–113 (2002).
20. D. Huang, E. A. Swanson, C. P. Lin, J. S. Schuman, W. G. Stinson, W. Chang, M. R. Hee, T. Flotte, K. Gregory, C. A. Puliafito, and J. G. Fujimoto, "Optical coherence tomography," Science **254**(5035), 1178–1181 (1991).
21. Z. Chen, T. E. Milner, S. Srinivas, X. Wang, A. Malekafzali, M. J. C. van Gemert, and J. S. Nelson, "Noninvasive imaging of in vivo blood flow velocity using optical Doppler tomography," Opt. Lett. **22**(14), 1119–1121 (1997).
22. R. Leitgeb, L. Schmetterer, W. Drexler, A. Fercher, R. Zawadzki, and T. Bajraszewski, "Real-time assessment of retinal blood flow with ultrafast acquisition by color Doppler Fourier domain optical coherence tomography," Opt. Express **11**(23), 3116–3121 (2003).
23. B. White, M. Pierce, N. Nassif, B. Cense, B. Park, G. Tearney, B. Bouma, T. Chen, and J. de Boer, "In vivo dynamic human retinal blood flow imaging using ultra-high-speed spectral domain optical coherence tomography," Opt. Express **11**(25), 3490–3497 (2003).
24. Y. Wang, B. A. Bower, J. A. Izatt, O. Tan, and D. Huang, "Retinal blood flow measurement by circumpapillary Fourier domain Doppler optical coherence tomography," J. Biomed. Opt. **13**(6), 064003 (2008).
25. Y. Wang, A. Fawzi, O. Tan, J. Gil-Flamer, and D. Huang, "Retinal blood flow detection in diabetic patients by Doppler Fourier domain optical coherence tomography," Opt. Express **17**(5), 4061–4073 (2009).
26. Y. Jia, O. Tan, J. Tokayer, B. Potsaid, Y. Wang, J. J. Liu, M. F. Kraus, H. Subhash, J. G. Fujimoto, J. Hornegger, and D. Huang, "Split-spectrum amplitude-decorrelation angiography with optical coherence tomography," Opt. Express **20**(4), 4710–4725 (2012).
27. B. Potsaid, B. Baumann, D. Huang, S. Barry, A. E. Cable, J. S. Schuman, J. S. Duker, and J. G. Fujimoto, "Ultrahigh speed 1050nm swept source/Fourier domain OCT retinal and anterior segment imaging at 100,000 to 400,000 axial scans per second," Opt. Express **18**(19), 20029–20048 (2010).
28. American National Standard for Safe Use of Lasers, ANSI Z136, 1–2007 (American National Standards Institute, New York, 2007).
29. N. Strouthidis, H. Yang, B. Fortune, J. Crawford Downs, C. Burgoyne, "Detection of optic nerve head neural canal opening within histomorphometric and spectral domain optical coherence tomography data sets," Invest. Ophthalmol. Vis. Sci. **50**(1), 214–223 (2009).
30. Z. Hu, M. D. Abràmoff, Y. H. Kwon, K. Lee, and M. K. Garvin, "Automated segmentation of neural canal opening and optic cup in 3D spectral optical coherence tomography volumes of the optic nerve head," Invest. Ophthalmol. Vis. Sci. **51**(11), 5708–5717 (2010).
31. N. G. Strouthidis, H. Yang, J. F. Reynaud, J. L. Grimm, S. K. Gardiner, B. Fortune, and C. F. Burgoyne, "Comparison of clinical and spectral domain optical coherence tomography optic disc margin anatomy," Invest. Ophthalmol. Vis. Sci. **50**(10), 4709–4718 (2009).
32. J. M. McDonnel, "Ocular embryology and anatomy," in *Retina*, S. J. Ryan, ed. (CV Mosby, St Louis, 1989), pp. 5–16.
33. S. Wolf, O. Arend, W. E. Sponsel, K. Schulte, L. B. Cantor, and M. Reim, "Retinal hemodynamics using scanning laser ophthalmoscopy and hemorheology in chronic open-angle glaucoma," Ophthalmology **100**(10), 1561–1566 (1993).
34. P. Hamard, H. Hamard, J. Dufaux, and S. Quesnot, "Optic nerve head blood flow using a laser Doppler velocimeter and haemorheology in primary open angle glaucoma and normal pressure glaucoma," Br. J. Ophthalmol. **78**(6), 449–453 (1994).
35. G. Holló, T. J. van den Berg, and E. L. Greve, "Scanning laser Doppler flowmetry in glaucoma," Int. Ophthalmol. **20**(1-3), 63–70 (1996-1997).
36. J. Kerr, P. Nelson, and C. O'Brien, "A comparison of ocular blood flow in untreated primary open-angle glaucoma and ocular hypertension," Am. J. Ophthalmol. **126**(1), 42–51 (1998).
37. K. M. Joos, L. E. Pillunat, R. W. Knighton, D. R. Anderson, and W. J. Feuer, "Reproducibility of laser Doppler flowmetry in the human optic nerve head," J. Glaucoma **6**(4), 212–216 (1997).

38. J. C. Hwang, R. Konduru, X. Zhang, O. Tan, B. A. Francis, R. Varma, M. Sehi, D. S. Greenfield, S. R. Sadda, and D. Huang, "Relationship among visual field, blood flow, and neural structure measurements in glaucoma," Invest. Ophthalmol. Vis. Sci. **53**(6), 3020–3026 (2012).
39. A. Mariampillai, B. A. Standish, E. H. Moriyama, M. Khurana, N. R. Munce, M. K. K. Leung, J. Jiang, A. Cable, B. C. Wilson, I. A. Vitkin, and V. X. D. Yang, "Speckle variance detection of microvasculature using swept-source optical coherence tomography," Opt. Lett. **33**(13), 1530–1532 (2008).
40. A. Mariampillai, M. K. Leung, M. Jarvi, B. A. Standish, K. Lee, B. C. Wilson, A. Vitkin, and V. X. Yang, "Optimized speckle variance OCT imaging of microvasculature," Opt. Lett. **35**(8), 1257–1259 (2010).

1. Introduction

Glaucoma is a leading cause of blindness [1,2] that is characterized by degeneration of the optic nerve associated with cupping of the optic nerve head (ONH). Although elevated intraocular pressure is often implicated, evidence, at least in some cases, shows that vascular insufficiency in the ONH also plays an important role in glaucoma [3].

The optic nerve head tissue is supplied by two main source of blood flow: the superficial layers of the optic nerve head (nerve fiber layer on the surface of the optic disc) by the central retinal artery (CRA) circulation; and the deeper layers (the prelaminar, lamina cribrosa, and retrolaminar regions) by the posterior ciliary artery (PCA) circulation [4]. Previous reports indicate that the primary site of ONH lesion in glaucoma is mainly nourished by the microcirculation of PCA [5,6]. Thus, it is critical that any method used to evaluate the role of the ONH circulatory disorders in glaucoma give reliable information about microcirculation [3].

Currently, a number of methods have been used for measuring ONH perfusion. Fluorescein angiography provides useful qualitative information in health and disease [7]; however, it only shows the superficial ONH vessels and does not assess deep ONH perfusion [8]. Additionally, injection of dye can cause nausea and anaphylaxis [9], making it unsuitable as a tool for routine glaucoma assessment. Both laser Doppler flowmetry, which samples capillary flow over a small retinal area [3,10–12], and laser speckle flowgraphy, which provides a spot sample of blood velocity [13], can show differences between glaucoma and normal group [14–17]. However the measurements provided by these methods are too variable for diagnostic application due to dependence on the signal strength and the location of the small sampled area. Magnetic resonance imaging (MRI) has been proposed to quantitatively image ONH perfusion; however, the major limiting factor with this method is the small size of the ONH and limited resolution to detect focal or mild circulatory insufficiency [18,19].

Optical coherence tomography (OCT) [20] is an imaging technique that has been widely used for diagnosis and management of ocular diseases. As a coherence detection technique, OCT can detect the Doppler frequency shift of the backscattered light that provides information on blood flow [21–23]. Doppler OCT has been used for measuring total human retinal blood flow (TRBF) around the ONH [24,25]. With this method, flow in the large vessels around the ONH can be quantified, but microcirculation of the ONH cannot be resolved because the velocities in the small vessels are too low to be accurately measured from Doppler shift. To measure local microcirculation, we recently developed the split-spectrum amplitude-decorrelation angiography (SSADA) algorithm that provides high quality three-dimensional (3D) angiography using ultrahigh speed OCT [26]. Because SSADA is based on the variation of reflectance amplitude, it is sensitive to motion and flow in all directions. This omnidirectional nature allow it to detect perfusion in a way that is independent of beam incidence angle [26]. Therefore SSADA may be a good basis for quantitative angiography of the ONH microcirculation.

In this article, we report the first use of OCT angiography to quantify human ONH blood flow. The ONH blood flow obtained from preperimetric glaucoma (PPG) patients was compared with the result from normal subjects. Our preliminary results indicate that 3D

quantitative OCT angiography could provide important information on glaucoma diagnosis and help predict the risk of progression.

2. Methods

2.1. Study population

The research adhered to the tenets of the Declaration of Helsinki in the treatment of human subjects. The study protocol was approved by Institutional Review Board (IRB). Four PPG patients (average ± standard deviation age 68 ± 7.1 years) and four normal subjects (57 ± 11.3 years) were recruited to participate in the study at Casey Eye Institute in Oregon Health & Science University (OHSU). One eye from each subject was scanned and analyzed. A PPG eye exhibits glaucomatous ONH rim defects or nerve fiber layer defects on ophthalmoscopy, but it does not have visual field defects meeting the diagnostic criteria for glaucoma. Standard eye examinations and visual field tests were performed on both eyes of the normal subjects. Detailed eligibility criteria and testing procedures can be found in the Manual of Procedures of the Advanced Imaging for Glaucoma study (www.AIGStudy.net).

2.2. System setup

The system used to quantify human ONH blood flow was similar to that used in our previous work [26,27]. To enhance the choroidal penetration and increase imaging depth, we used a swept light source with a central wavelength of 1050 nm. The laser wavelength sweep range was 100 nm with a full-width-half-maximum (FWHM) of 69 nm (Fig. 1, left), providing an axial resolution of 5.3 µm and an image depth range of 2.9 mm in tissue by assuming that the refractive index of the sample is ~1.33. The laser sweep repetition rate was 100 kHz. The emitted light from the laser was split into the sample and reference arms. In the sample arm, a focused spot of 18-µm FWHM amplitude was estimated on the retinal plane. Interference between light returning from the reference and sample arms was detected by a balanced receiver. The ocular light power exposure was 1.9 mW, which was within the American National Standards Institute (ANSI) safety limit [28].

The scanning protocol was optimized for the SSADA algorithm [26]. In the fast transverse scan (X) direction, the B-scan contained 200 A-lines covering 3 mm. With this configuration, the B-scan frame rate of the system was 476 frames per second. In the slow transverse scan (Y) direction, 200 sampling positions covering 3 mm were used to capture a 3D data set, with 8 repeated B-scans at every position. The 8 repeated B-frames (M-B frames, Fig. 1, left) were used for the SSADA calculation to obtain both the structure and blood flow images. Therefore, 1,600 B-scans were acquired to form a 3D data cube within an acquisition time of 3.4 seconds.

2.3. Data acquisition

After pupil dilation with 1% tropicamide and 2.5% phenylephrine eyedrops, the subject's head was stabilized by chin and forehead rests. A flashing internal fixation target was projected by an attenuated pico projector using digital light processing technology. The imaging area on the fundus was visualized by the operator using a real-time *en face* view of a 3 mm × 3 mm OCT preview scan. Four angiography scans were consecutively obtained in one session.

2.4. Data processing

2.4.1. SSADA

The basic procedures of SSADA are shown in Fig. 1. The key step of SSADA is splitting the raw full spectrum into multiple spectrums, each with a narrow bandwidth. Narrower bandwidths were intentionally created to lower the OCT axial resolution. This minimized the pulsatory bulk motion noise along the axial direction and optimized flow detection along the

transverse direction. After the narrower spectra were Fourier-transformed, low resolution OCT amplitude frames were used to calculate decorrelation. Inter-B-scan decorrelation could be determined at each of the narrower spectral bands separately and then averaged. Recombining the decorrelation images from the multiple narrow spectral bands yielded high quality cross-sectional angiograms (Fig. 1, right) that used the full information in the entire OCT spectral range.
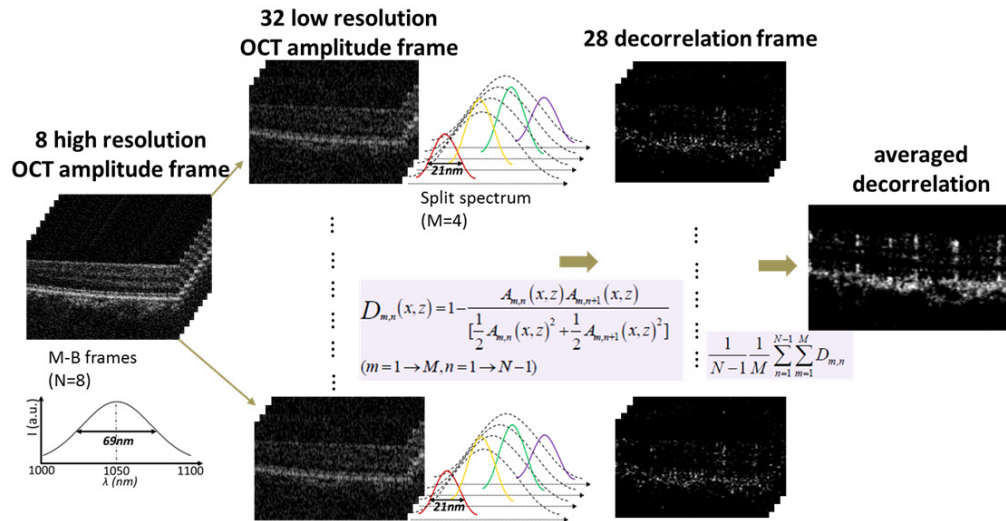

Fig. 1. Flow chart detailing the basic steps of the SSADA algorithm. Eight OCT M-B frames were scanned consecutively at the same spatial location to produce 8 spectral interferograms and 8 standard-resolution cross-sectional images. In conventional decorrelation angiography, decorrelation is calculated between these standard resolution images, but this produces a low-quality angiogram. In SSADA, each full spectral interferogram was split into 4 spectral bands. There were 8 OCT image frames at each spectral band, from which 7 decorrelation frames were calculated. The 28 decorrelation frames were averaged to produce one final decorrelation-based flow cross-section of much higher quality [26].

The decorrelation (D) can be simply considered as the fluctuating values of OCT intensities. To be specific, the blood flow results in fluctuation in the amplitude of OCT fringes as RBCs enter and exit a particular voxel. Hence the eight M-B frames contain fluctuating values of OCT output intensities at any given voxel in the flow of blood, and the definition of D is constructed so that fluctuating intensities yield high D values (approaching 1.0). Pixels in the M-B frames that contain static tissue and hence constant intensities yield small D values (approaching 0). In SSADA result, D is a function of the flow velocity regardless of direction, given the RBCs concentration is constant [26]. The faster blood particles move across the laser beam, the higher D of the received signals within a velocity range set by the scan parameters. In the other words, D is proportional to flow velocity, but it can be saturated at the maximum detectable flow velocity, due to a limit of time resolution for each scan parameters [26].

2.4.2. Detection of optic disc boundary

Two hundred cross-sectional reflectance intensity images (Fig. 2(A)) and decorrelation (flow) images (Fig. 2(B)) could be summarized and viewed as *en face* maximum projections (Figs. 2(C), 2(D)). The projection algorithm found the maximum reflectance and decorrelation value for each transverse position, representing the highest reflectance and fastest flowing vessel lumen respectively. We used the neural canal opening (NCO), which is the termination of the retinal pigment epithelium (RPE)/Bruch's membrane (BM) complex [29,30], to define the ONH margin [31]. In OCT cross-sectional B-scans, the boundary of the NCO, indicated by

two green dashed lines (Fig. 2(E)), was determined by the termination of the RPE/BM complex (two green arrows). It corresponded to the two margin points at the disc region. These representative margin points were transferred to the corresponding flow cross-sectional image (Fig. 2(F)) and *en face* projection maps (Figs. 2(C), 2(D)). Apparently, the boundary produced by the surrounding peripapillary choroidal blood flow in the flow data cannot be used as the detection method for disc margin.
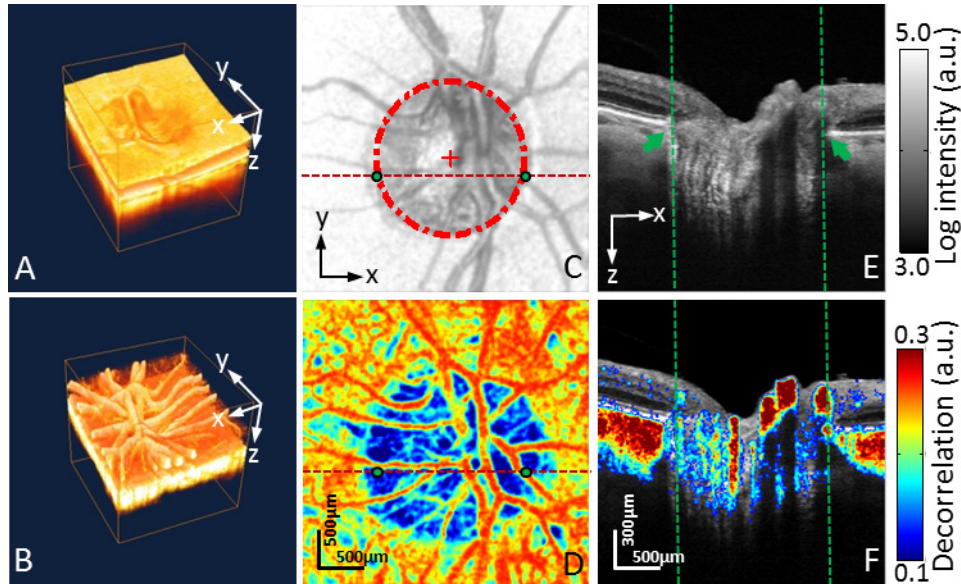

Fig. 2. *In vivo* 3D volumetric [3.0 (x) × 3.0 (y) × 2.9 (z) mm] OCT images of the ONH in the right eye of a normal subject. The images in (E) and (F) were cropped from 2.9 mm to 1.8 mm axially. (A) Rendering of a scanned disc volume reflectance intensity image . (B) 3D rendering of flow image. (C) An *en face* maximum reflectance intensity projection showed branches of the central retinal vessels. (D) *En face* maximum decorrelation projection angiogram. (E) OCT cross-section at the plane marked by red dashed line in (C). The boundary of the neural canal opening (NCO), indicated by two green dashed lines, was determined by the termination of the RPE/BM complex, shown by two green arrows that corresponded to the two margin points in (C) & (D). (F) Cross-sectional gray scale reflectance intensity image overlaid by the color scale flow (decorrelation) image shows that the abundant ONH circulation resides mainly in the lamina cribosa region. The ONH blood flow was obviously lower than that of the major retinal vessels and choroidal vessels, but it was clearly shown in the maximum projection map (see the temporal section of (D)).

Because the NCO was detectable, it was manually delineated on the reflectance projection image (Fig. 2(C), red dashed ellipse). The major and minor axes of the ellipse were then calculated along the vertical and horizontal directions. The approximate center of disc was the centroid of the selected ellipse.

2.4.3. Quantification of flow index and vessel density

After the position and dimensions of a disc were determined, the whole disc and temporal ellipse areas were segmented for quantitative analysis. The optic disc mask was idealized as an ellipse with vertical diameter (VD) and horizontal diameter (HD) (Fig. 3(B1)). The mask value was 1 inside the ellipse and 0 outside. We also defined an elliptical mask for the disc region temporal to the major superior and inferior branch arteries and veins. The temporal ellipse had a major axis diameter of 0.75 VD and a minor axis diameter of 0.50 HD (see Fig. 3(B2)). The temporal ellipse was tilted inferiorly to fit the tilt of the disc vessel pattern associated with the tilt of the disc-fovea axis. According to the literature measurements on the normal population [32], the average value of this angle is 7.1° (Fig. 3(B2)). The temporal

ellipse region did not contain any major branch retinal blood vessels and therefore was a better measure of local disc microcirculation. By multiplying two different masks with the original blood flow projection map, respectively, the segmented flow maps (Figs. 3(C1), 3(C2)) were acquired for further quantification.
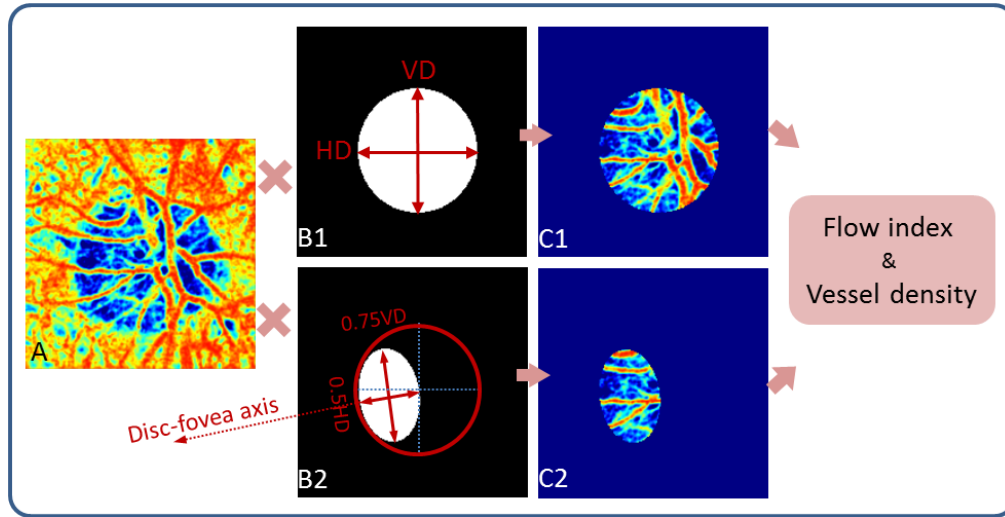

Fig. 3. Flow chart displaying extraction of the flow regions for quantification. (A) The *en face* maximum decorrelation projection angiogram. The color scale (decorrelation) was related to the localized blood flow magnitude. (B1) The whole disc mask with known value of VD and HD, created by the method described in section 2.4.2. (B2) The temporal elliptical area, derived from the primary whole disc ellipse. The arrow indicates the tilted angle based on the disc-fovea axis. (C1) and (C2) Final segmented flow maps, achieved by multiplying the original disc flow map (A) with two different disc masks (B1 and B2). Further processing could be applied for quantification.

The flow index was defined as the average decorrelation values in the segmented area given by

$$\frac{\int_A D \cdot V dA}{\int_A dA} \quad (V = 1, \text{ if vessel}; V = 0, \text{ if not}), \tag{1}$$

where A is the disc area or the temporal ellipse area within the disc, and D is the decorrelation value acquired by SSADA. The essential definition of D was shown in the central panel of Fig. 1, where N is the number of M-B frames (N = 8) and M is the number of split spectrum (M = 4).

The vessel density was defined as the percentage area occupied by vessels in the segmented area, using the following formula:

$$\frac{\int_A V dA}{\int_A dA} \quad (V = 1, \text{ if vessel}; V = 0, \text{ if not}), \tag{2}$$

where A is the disc area or the temporal ellipse area within the disc. The threshold decorrelation value used to judge V as 1 or 0 was set at 0.125, two standard deviations above the mean decorrelation value in the noise region. Before calculation of the decorrelation values by SSADA, the central foveal avascular zone in normal eyes was chosen as a noise region after we applied the same scanning pattern on the macular region.

2.5. Statistical analysis

The mean and standard deviation (SD) were calculated from four scans of each subject, and the coefficient of variation (CV) was calculated to assess repeatability. Unpaired t-tests were used to compare the parameters of flow index and vessel density between normal and PPG, assuming unequal variance.

3. Results

3.1. Quality control of decorrelation values

Before we could obtain useful flow index measurements, we needed to minimize the signal strength effect in some cases. If the subject lost the fixation target when the ONH was being scanned, the light source was partially or totally blocked by the edge of the pupil. Therefore noise predominates in pixels with low OCT signal amplitude and therefore flow cannot be assessed in these pixels with any accuracy. In SSADA algorithm, we assign zero decorrelation values to pixels in the decorrelation frame where the respective pixels in the amplitude frame have subthreshold amplitude value. Consequently the angiography results will be biased by the signal strength lower than noise floor (threshold).
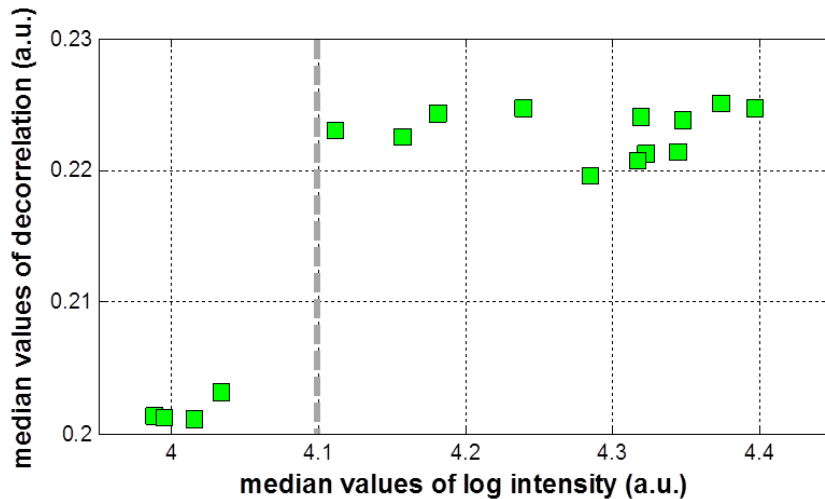

Fig. 4. Relationship between reflectance intensity and decorrelation used for quality control of 3D decorrelation values. The median values of log intensity and median values of decorrelation were acquired through two 3D outputs (reflectance intensity/decorrelation). All of the values were collected from 4 normal subjects (16 scans). This plot indicates 4.1 (log intensity) can be considered as the cutoff point to remove the scans with lower intensity values that would bias the resulting decorrelation/flow values.

In this study, we established quality control by removing scans with insufficient signal strength. To evaluate the relationship between signal strength and flow strength, we obtained the median values of the log intensity and median values of the decorrelation through two 3D outputs (reflectance intensity/decorrelation). We plotted these two types of values acquired from all scans of 4 normal subjects (16 scans, Fig. 4). We found that when the median value of log intensity was lower than 4.1, the median values of decorrelation were reduced by ~10% for the whole scan volume. In contrast to the outliers at left side, decorrelation values were constant when the median value of the log intensity was over 4.1, as shown by the 12 scans at right side of Fig. 4. Therefore, in this study 4.1 was determined as the cutoff point for the quality control. No scans with a median value of log intensity lower than 4.1 were considered for quantification. After this quality control step, 3 patients and 3 normal subjects were left for the following study.

3.2. Comparison on visualization

OCT angiography provided detailed ONH microcirculation structural and flow imagery for both normal and PPG patients. The maximum projection images of ONH vascular perfusion from representative normal subjects and PPG patients are shown in Figs. 5(B), 5(D), along with the disc photographs in Figs. 5(A), 5(C). Disc photographs clearly demonstrated the major retinal branch vessels, but it was almost impossible to identify the microcirculations and provide flow information. The ONH angiogram obtained by the SSADA algorithm showed many orders of vascular branching and the microcirculatory network in the peripapillary regions (Figs. 5(B), 5(D)). In normal subjects, a dense microvascular network was visible on OCT angiograms of the ONH (Fig. 5(B)). This network was visibly attenuated in all PPG subjects (Fig. 5(D)). Obviously, this difference could not be visualized by disc photographs.
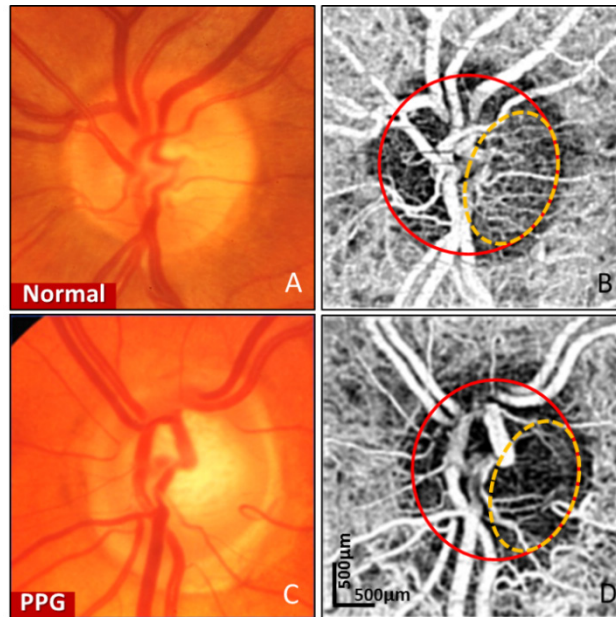

Fig. 5. Disc photographs (A, C) and *en face* OCT angiograms (B, D) of the ONH in representative normal (A, B) and preperimetric glaucoma (PPG) subjects (C, D). Both examples are from left eyes. In (B) and (D) the solid circles indicate the whole discs, and the dash circles indicate the temporal ellipses. A dense microvascular network was visible on the OCT angiography of the normal disc (B). This network was greatly attenuated in the glaucomatous disc (D).

3.3. Comparison of flow index and vessel density

To obtain disc perfusion measurements of the different disc regions, the flow index and vessel density were calculated at selected disc areas according to Eqs. (1) and (2), respectively, in each scan of each subject. Analysis of results acquired from the whole discs of the 3 normal subjects and 3 PPG patients showed that the flow index was reduced by 35% and the vessel area was reduced by 34% in the PPG group ($p < 0.05$ each, Table 1). The repeatability as assessed by the CV was 6.8% and 6.2% for flow index and vessel density, respectively.

Table 1. OCT disc perfusion measurements on the whole disc region[a]

Parameters	Normal	PPG	p-value	CV (%)
Flow index (dimensionless)	0.160 ± 0.031	0.104 ± 0.009	0.040	6.81
Vessel density (%)	74.2 ± 14.3	49.1 ± 5.20	0.045	6.23

[a]PPG, preperimetric glaucoma; CV, coefficient of variation of repeated measurements; p-values based on unpaired t-tests.

Regional disc perfusion measurements based on the temporal ellipse of the disc showed that both the flow index and the vessel density were reduced by 57% in the PPG group (p ~ 0.01 each, Table 2). Thus, the estimated reductions were higher than those based on the whole disc region. For this small region quantification, the repeatabilities of the measurements of flow index and vessel density were 9.0% and 8.4%, respectively. The population coefficient of variation was 13% and 42% for normal and PPG groups, respectively.

Table 2. OCT disc perfusion measurements on the temporal ellipse of the disc[a]

Parameters	Normal	PPG	p-value	CV (%)
Flow index (dimensionless)	0.150 ± 0.020	0.064 ± 0.027	0.010	9.04
Vessel density (%)	72.7 ± 9.61	31.5 ± 13.6	0.013	8.42

[a]PPG, preperimetric glaucoma; CV, coefficient of variation of repeated measurements; p-values based on unpaired t-tests.

4. Discussion

Using OCT angiography, we have shown that ONH blood flow can be determined in both normal and glaucoma groups. We targeted two regions, the whole disc and a temporal ellipse area within the disc, for comparison between two groups. By excluding the major superior and inferior branches of the retinal vessels on the temporal side, we focused our quantifications mainly on ONH microvascular beds. Our preliminary results suggest that in early glaucoma the reduction of ONH microvascular flow is much more dramatic than that of whole ONH circulation. This suggests that quantification performed on microvascular perfusion may be more sensitive for detecting ONH circulatory changes in early glaucoma patients.

Our results confirm the finding of several other techniques that reported a significantly reduced ONH perfusion in glaucoma. Using fluorescein angiography, Wolf demonstrated that glaucoma is associated with an increased arteriovenous passage time and a decreased fluorescein velocity [33]. Using single-point laser Doppler flowmetry, a few authors similarly reported decreased blood flow in the ONH of glaucoma and glaucoma suspects when compared with normal subjects [14,34]. Using scanning laser Doppler flowmetry, Michelson reported that both neuroretinal rim blood flow and peripapillary retinal blood flow were significantly decreased in glaucoma patients compared with controls [15]. Hafez also found open-angle glaucoma patients have lower blood flow in the ONH and suggested perfusion might be reduced before the manifestation of visual field defects [16]. Conversely, Hollo failed to detect a significant difference in neuroretinal rim blood flow in their population of glaucoma patients compared with control subjects [35]. By use of laser speckle flowgraphy, Sugiyama's group reported less blood flow was observed at the superior and inferior sectors of the ONH rim in patients with PPG compared to normal control subjects [17]. Overall, previous results agree with our finding that ONH perfusion is reduced in glaucomatous eyes.

In previous reports, the temporal sector has been studied separately for evaluating glaucoma patients' disc perfusion. Kerr reported reduced blood flow in the lamina cribrosa and the temporal neuroretinal rim of the ONH of glaucoma patients in comparison with ocular hypertensives [36]. Sugiyama reported the blood flow became reduced at the temporal sectors as open angle glaucoma progressed compared to patients with PPG [17]. Our finding via OCT angiography also confirmed that the temporal sector is a critical study region for monitoring progression of glaucoma patients. Although the repeatability of the temporal disc measurements is not quite as good as whole disc measurements, it is still better than that of laser Doppler flowmetry [37]. Using Doppler OCT with dual-circular scans, our group previously found TRBF was reduced by ~30% in patients with perimetric glaucoma in which eyes have significant glaucomatous visual field damage [38]. In this pilot study, we found that the angiography-based flow index was reduced by 35% for the whole disc and by 57% for the temporal ellipse area of the disc in a group of PPG subjects. Our results indicate that the reduction in ONH flow in PPG patients may be more dramatic than reductions in TRBF.

Thus, reductions in ONH blood flow detectable by OCT angiography precede detectable visual field damage, suggesting it could be useful in the early detection of glaucoma and the evaluation of glaucoma progression risk.

It should be noted that the amplitude-based method that we have developed is sensitive to motion that is perpendicular (transverse flow) or parallel (axial flow) to the OCT beam. We believe this characteristic of SSADA makes quantitation of microvascular flow independent on beam incidence angle. In addition, we chose to compute amplitude decorrelation rather than amplitude variance (also called speckle variance) [39,40] because decorrelation is less affected by signal strength (i.e., variation due to media scattering, pupil blocking, focusing, polarization mismatch, etc.). This is important because previous techniques such as the laser Doppler flowmetry could not reliably compare flow values between individuals due to the effect of signal strength on the measurements [3,10–12].

Quantitative SSADA has several limitations. First, flow projection artifact from superficial blood vessels to deeper tissue levels prevents us from separately measuring superficial and deep ONH flow. The artifact is caused by the moving shadow cast by flowing blood cells. Decorrelation is caused by both moving reflectors (blood cells) and moving shadows (projected on distal high reflectance tissue). The two type of decorrelation is not distinguished by SSADA – both appear as flow in the 3D angiogram. The artifact is not problematic if our analysis is confined to the 2D maximum projection angiogram. Therefore the study was limited to the use of 2D angiograms that measured superficial and deep vascular beds together. Second, the ONH flow index includes measurements on both local disc circulation and large retinal blood vessels. Thus it is a mixture of both disc and retinal circulation and not a pure measurement of a single vascular bed. However, since glaucoma and optic nerve diseases reduce both circulations, the mixed measurement is clinically useful. Third, OCT angiography cannot distinguish between perfusion reduction caused by tissue loss (a result of glaucoma) and ischemia (a cause of glaucoma). However, the OCT structural images can measure tissue loss. Thus, structural imagery and perfusion measurements could provide complementary information for both clinical assessment and pathophysiological investigation.

5. Summary

We used OCT angiography and the new SSADA algorithm to generate *in vivo* measurements of ONH blood flow. Flow indices and vessel densities in the segmented disc areas and temporal sections were measured in PPG patients and normal control subjects. The reductions of these two flow parameters in the two different areas were statistically significant. Our results showed that OCT angiography was able to detect reduced ONH perfusion in a small group of early glaucoma patients. Further studies are needed to assess the potential of this new technology in glaucoma diagnostic and prognostic evaluation.

Acknowledgments